ACS PHYSICAL CHEMISTRY Au
AN OPEN ACCESS JOURNAL OF THE AMERICAN CHEMICAL SOCIETY

pubs.acs.org/physchemau

Article

Excitonic Nature of Carotenoid–Phthalocyanine Dyads and Its Role in Transient Absorption Spectra

Vladislav Sláma,* Lorenzo Cupellini, and Benedetta Mennucci*

Cite This: *ACS Phys. Chem Au* 2022, 2, 206–215

Read Online

ACCESS | Metrics & More | Article Recommendations | Supporting Information

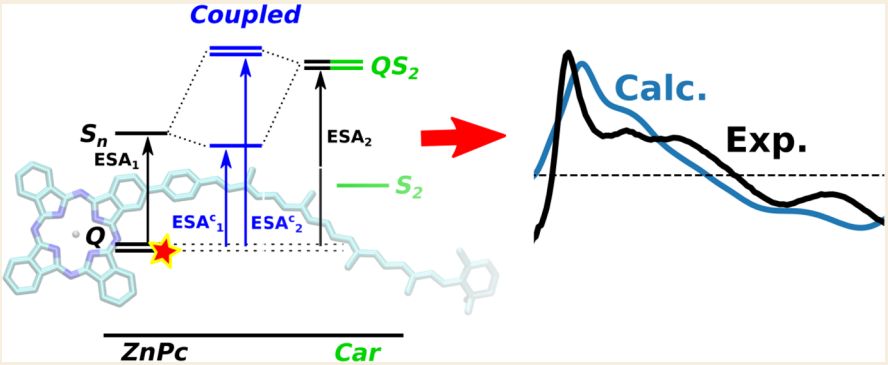

ABSTRACT: Artificial carotenoid–tetrapyrrole dyads have been extensively used as model systems to understand the quenching mechanisms that occur in light-harvesting complexes during nonphotochemical quenching. In particular, dyads containing a carotenoid covalently linked to a zinc phthalocyanine have been studied by transient absorption spectroscopy, and the observed signals have been interpreted in terms of an excitonically coupled state involving the lowest excited states of the two fragments. If present, such excitonic delocalization would have significant implications on the mechanism of nonphotochemical quenching. Here, we use quantum chemical calculations to show that this delocalization is not needed to reproduce the transient absorption spectra. On the contrary, the observed signals can be explained through excitonic couplings in the higher-energy manifold of states. We also argue that the covalent linkage between the two fragments allows for electronic communications, which complicates the analysis of the spectra based on two independent but coupled moieties. These findings call for a more thorough reassessment of the photophysics in these dyads and its implications in the context of natural nonphotochemical quenching.

KEYWORDS: *transient absorption, nonphotochemical quenching, energy transfer, excitonic coupling, artificial light-harvesting dyad*

INTRODUCTION

In the light-harvesting (LH) process of plants, chlorophylls play the major role as they are responsible for light absorption and energy transfer to the reaction center. However, the absorption efficiency of the chlorophyll-containing LH complexes is further increased by the copresence of carotenoids (Cars) which absorb light at a higher frequency than chlorophylls thus enlarging the region of the visible spectrum that can be exploited.[1] In addition, the interactions between chlorophylls and Cars are believed to be responsible for the protective mechanisms which are activated in high light conditions. These mechanisms are collectively called non-photochemical quenching (NPQ).[2−7] The precise nature of the processes involved in NPQ is still under debate and might vary from one system to another.[8] Investigating these processes in natural LH complexes has proven to be a very challenging task due to the large number of different interactions and processes involved, including conformational changes of the whole complex.[9−13]

A promising strategy is thus to study how carotenoids induce quenching processes in artificial systems that mimic the function of natural light-harvesting complexes, such as chromophore dyads.[14] In these systems, the interacting chromophores, usually a carotenoid and a tetrapyrrole equivalent of chlorophylls,[15−21] are chemically linked rather than kept close by the protein scaffold. This makes artificial dyads simpler and more controllable systems as well as possible building blocks of bioinspired artificial light-harvesting devices.

In this work, we focus on dyads composed of a zinc phthalocyanine (ZnPc), a carotenoid (Car), and either a phenyl (Ph) or phenylamino (PhA) linker. These specific

Received: December 13, 2021
Revised: January 13, 2022
Accepted: January 18, 2022
Published: February 3, 2022

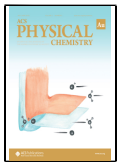

https://doi.org/10.1021/acsphyschemau.1c00049
ACS Phys. Chem Au 2022, 2, 206–215

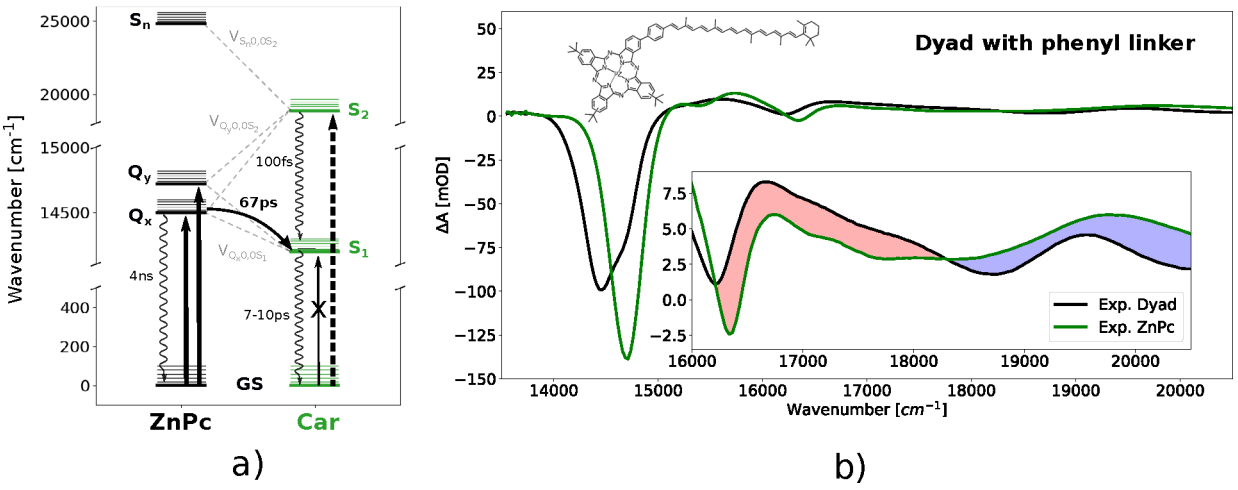

Figure 1. (a) Energy scheme and experimental lifetimes for the excited states of ZnPc (black) and Car with 10 DB (green). The solid vertical arrows represent the excitation from the ground state by the excitation pulse. (b) Experimental transient absorption spectra of **Dyad-Ph** at 2 ps waiting time excited at 680 nm, which are compared to the spectra of ZnPc, both measured in the toluene solvent. The difference between the spectra (filled surface) is usually interpreted as a signature of the Car S_1 state. The spectra have been taken from ref 21.

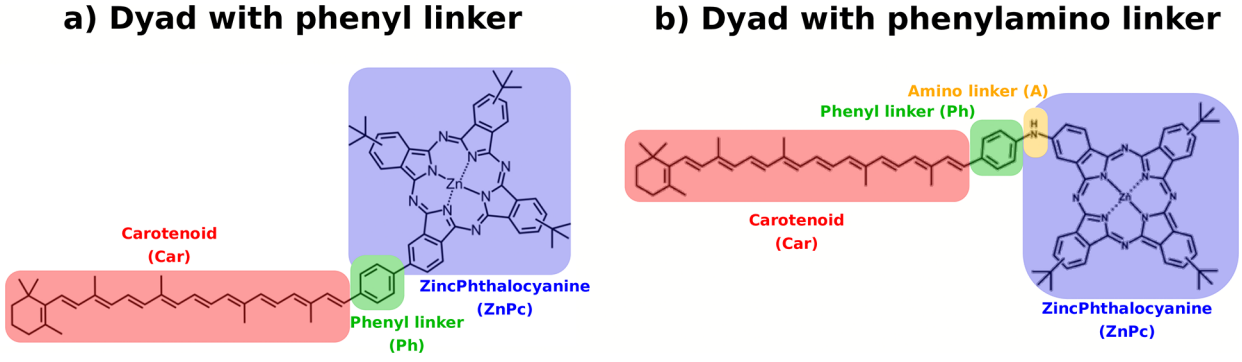

Figure 2. Fragments of the dyad with phenyl linker (**Dyad-Ph**) and phenylamino linker (**Dyad-PhA**).

dyads have been extensively studied through optical linear and nonlinear spectroscopy.[16,17,19−21] In both dyads, the initial excitation on the ZnPc moiety is quenched by the linked Car, as elucidated by transient absorption (TA) spectra.

The TA spectra and the implied dynamics of ZnPc−Car dyads are generally interpreted in terms of a model made of two independent but interacting fragments. When comparing the isolated ZnPc molecule to the dyad, a significant reduction of the excited-state lifetime is observed.[16,21] This quenching is explained by excitation energy transfer (EET) from the lowest Q state localized at the ZnPc moiety to the lowest (S_1) dark state localized in the Car moiety, from which a fast relaxation to the ground state is obtained (see Figure 1a).

The differences between the dyad and the ZnPc molecule are seen not only in the lifetime but also in the TA spectral shape. Figure 1b presents the TA spectra of a dyad with the phenyl linker and ZnPc after the selective excitation of the Q band. Both TA spectra are characterized by a sharp negative band, which arises from the ground-state bleaching (GSB) and stimulated emission (SE) of the Q bands of ZnPc. In addition, a broad positive signal at higher frequencies is present in both TA spectra, arising from excited-state absorption (ESA) from the lowest Q state. In the dyad, the Q band (at ca. 14 700 cm^{-1}) is broader and red-shifted with respect to the isolated ZnPc. In addition to the spectral changes of the Q band, the TA spectrum of the dyad presents a larger intensity with respect to the isolated ZnPc in the spectral region 16 000−18 300 cm^{-1} and a lower intensity for frequencies larger than 18 300 cm^{-1}. This difference, represented as a filled area in Figure 1, is generally ascribed to the TA signal from the Car S_1 state, due to the similarity to the S_1 signal obtained by selective excitation of the isolated carotenoid.[21] The carotenoid S_1 signal is characterized by a negative GSB of the $S_0 \rightarrow S_2$ absorption and an ESA contribution from S_1 at lower frequencies. Exciton mixing between Q and S_1 states would be experimentally observable through a signal similar to the S_1 one, with a positive ESA contribution at lower frequencies and a negative GSB at higher frequencies. This signal is present in the TA spectra immediately after the excitation without a measurable rise-time and decays with the lifetime of the ZnPc Q states. These properties, together with the bidirectional EET, are considered to be clear proof of exciton delocalization between ZnPc Q states and the Car S_1 state.[17,20,22] A similar picture is found for a similar dyad with a phenylamino linker.[16,19]

This interpretation implies a precise resonance condition between the Car S_1 state and the ZnPc Q states, whose energies have to match perfectly to make up for the small electronic coupling between them.[22,23] However, this signal is present for dyads with carotenoids characterized by different conjugation lengths.[16] As the S_1 excitation energy of the Car is strongly dependent on the length of the conjugated chain,[1,24]

https://doi.org/10.1021/acsphyschemau.1c00049
ACS Phys. Chem Au 2022, 2, 206−215

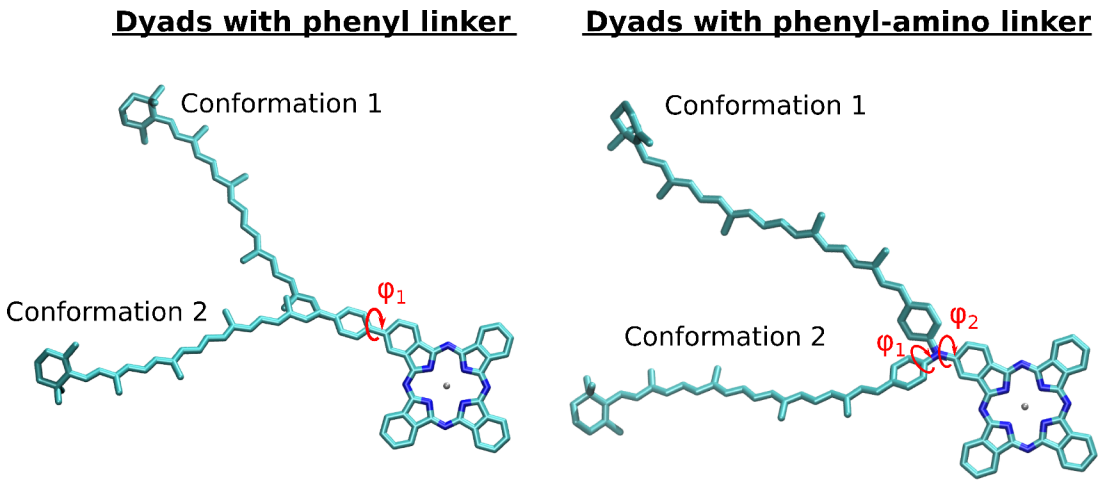

Figure 3. Different conformations of the dyads with a phenyl and phenylamino linker. The dihedral angles used for the relaxed scan are visualized in red.

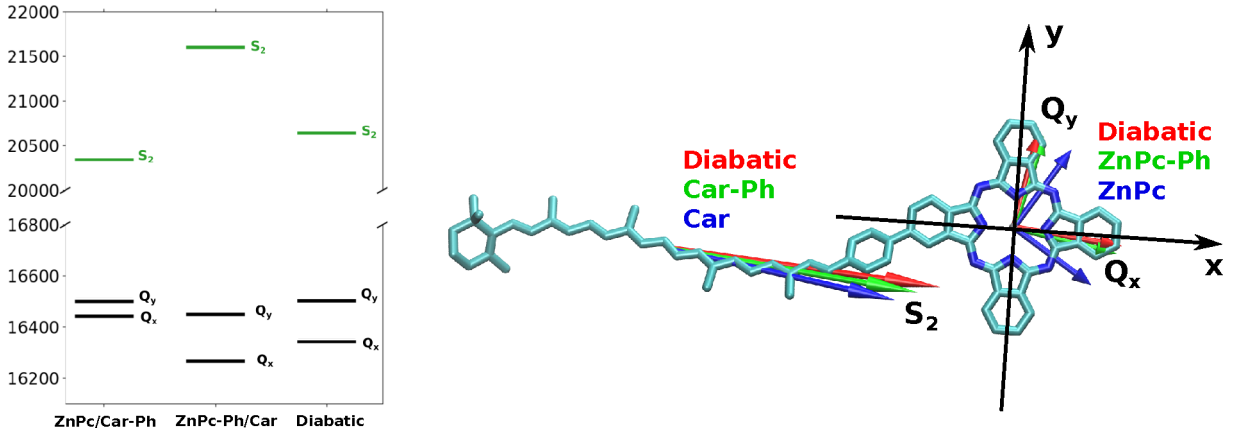

Figure 4. (left) Vertical excitation energies and transition dipoles for different fragmentation schemes, where the phenyl linker is included in either the ZnPc (**ZnPc-Ph**) or the Car fragment (**Car-Ph**), compared with the diabatic states. (right) Orientation of the transition dipoles of the three diabatic states of the dyad (Q_x, Q_y, and S_2) and the corresponding ones in the two isolated fragments with or without the inclusion of the linker.

one wonders how this resonance condition can be met for Cars of different conjugation lengths. It seems that this resonance should be present only at a specific S_1 energy, i.e., at a precise conjugation length. Despite this contradiction, the interpretation of the observed signal as an exciton mixing between ZnPc Q states and the Car dark S_1 state is generally accepted.[21,22]

In this study, we have used quantum chemical calculations to reveal the real nature of the observed signal in the difference TA spectra by investigating two covalent dyads composed of ZnPc, a carotenoid with 10 conjugated double bonds (10 DB) and a linker made of a phenyl group (Ph) and a phenylamine group (PhA), separately (see Figure 2). These molecules are henceforth termed **Dyad-Ph** and **Dyad-PhA**. This analysis is performed in two steps. First, we simulate the linear and transient absorption spectra of the dyads including only the bright S_2 state for the Car, and then, we estimate the effect of the dark S_1 state both on the TA spectra and on the excitation energy transfer.

Our calculations reproduce the measured changes in TA spectra upon passing from ZnPc to the dyad without the need to include the S_1 state. The observed signals in fact arise from the mixing within the higher-energy manifold of states that shape the excited-state absorption of the dyad. On the contrary, the mixing between the Q and S_1 states is negligible, owing to the large vibronic coupling in the S_1 state of the Car. However, this vibronic coupling does not hinder the $Q \rightarrow S_1$ energy transfer and consequent fluorescence quenching.

RESULTS AND DISCUSSION

Fragmentation of the Dyad

From a conformational analysis, we have identified two stable conformations for each of the two dyads (Figure 3). From the Boltzmann factors obtained at room temperature from the free energies calculated in toluene solution (see the Computational Details section), we find that the dyads exist in the two conformations with probabilities of 65% and 35% for **Dyad-Ph** and 68% and 32% for **Dyad-PhA**. If not stated otherwise, the analysis will be performed on the more stable conformation (conformation 2).

Having determined the structure of the dyads, we can start addressing the interpretation of the spectra using the Frenkel exciton model built on the two independent but interacting monomers (Car and ZnPc). However, here, the monomers are very close together and connected by a phenyl (Ph) or phenylamino (PhA) linker. The choice of the individual fragments is thus not straightforward; for example, the linker can be alternatively included in the Car fragment or in the

https://doi.org/10.1021/acsphyschemau.1c00049
ACS Phys. Chem Au 2022, 2, 206−215

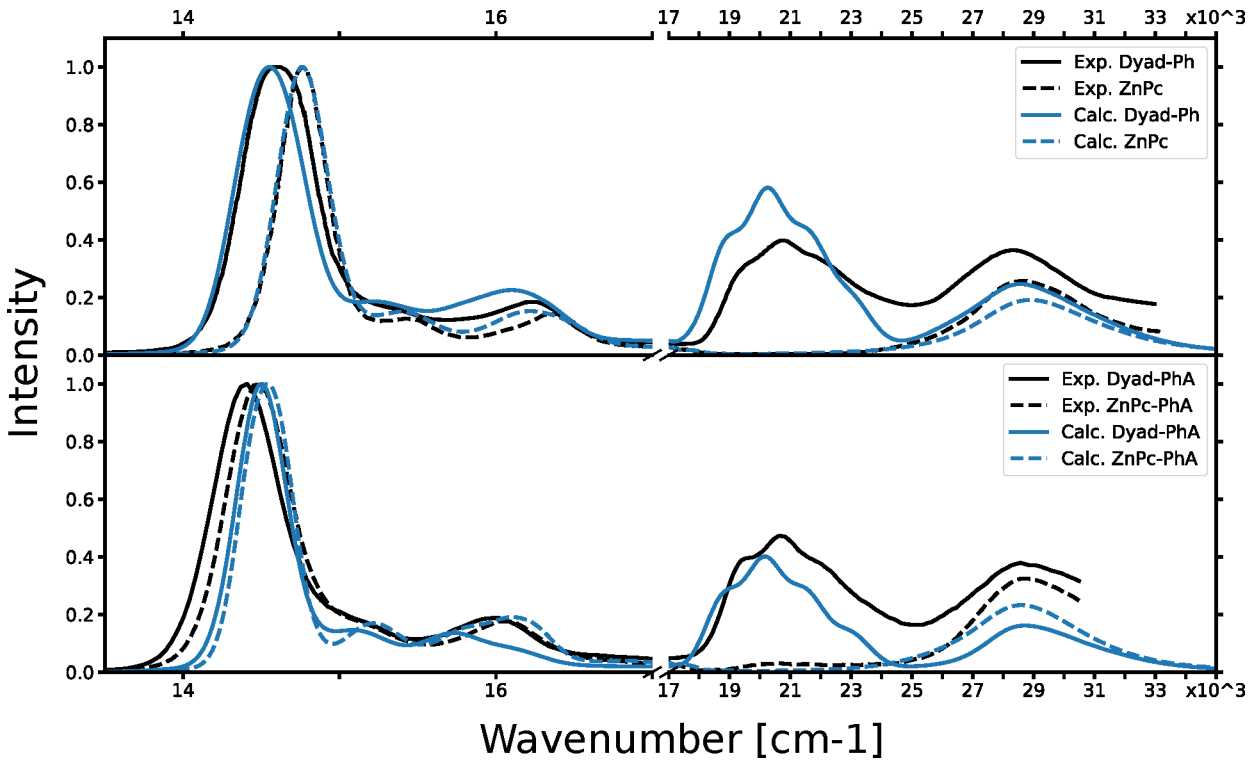

Figure 5. Comparison between experimental and calculated absorption spectra for **Dyad-Ph** (upper panel) and **Dyad-PhA** (lower panel) in toluene. The computed spectra are represented by blue lines and the experimental ones in black. The solid lines correspond to the dyads and the dashed ones to the corresponding monomers, ZnPc and **ZnPc-PhA**, respectively.[16,21] The dyad spectra were computed within the Frenkel exciton model with overlapping fragments (see the text).

ZnPc one. To identify the best fragmentation scheme, we performed a diabatization of the dyad's lowest excited states (see the Computational Details section), and then, we used the obtained diabatic states to test the different fragmentation schemes.

We note that when the diabatization is performed by cutting the single bond between the Ph linker and ZnPc, the resulting diabatic states (Q_x, Q_y, and S_2) and the couplings well describe the excited states of the full QM dyad (Table S1 of the SI). We can therefore use these diabatic states to check which fragments provide the best description of the dyad. Two sets of model systems were created by cutting the dyad at the linker and including the linker in either the ZnPc (**ZnPc-Ph**) or the Car (**Car-Ph**) fragment. From the data reported in Figure 4 (and Table S2 in the SI), it is clear that neither of these two model systems reproduce all of the dyad diabatic states. However, each model gives good results for a subset of states: S_2 for **Car-Ph** and Q_x and Q_y for **ZnPc-Ph**. The explanation of this behavior is simple. On one hand, the Ph linker extends the Car conjugation length and therefore needs to be included with the Car fragment to obtain a proper description of its S_2 excitation energy. On the other hand, the Ph linker contributes to the delocalization and energetic separation of the Q_x and Q_y transitions even if the ring is slightly rotated with respect to the ZnPc π-conjugation plane. Including the linker in ZnPc also improves the length and orientation of the transition dipoles (Figure 4), bringing them closer to those of the diabatic states of the dyad. In light of these results, the following exciton analysis will be based on two interacting and overlapping fragments where the linker is included with both Car and ZnPc (from now on, the exciton dyad).

To confirm that the excited states of these overlapping fragments represent the correct basis for the exciton model, the exciton couplings V between Q_x/Q_y and S_2 transitions were computed by the transition density cube (TDC) method[25] and compared with the couplings obtained from the diabatization of the dyad states (see the Computational Details section for details). The calculated exciton couplings $V^{\mathrm{TDC}}_{Q_x-S_2}$ = 529 cm^{-1} and $V^{\mathrm{TDC}}_{Q_y-S_2}$ = 184 cm^{-1} are similar to those obtained from the diabatization procedure, $V^{\mathrm{diab}}_{Q_x-S_2}$ = 497 cm^{-1} and $V^{\mathrm{diab}}_{Q_y-S_2}$ = 115 cm^{-1}.

As a final test, we computed the exciton spectra and compared them with the experimental absorption of the two dyads[19,21] (Figure 5). To have a more complete analysis, we also compared the calculated and experimental spectra of the isolated ZnPc and **ZnPc-PhA** molecules.

For **Dyad-Ph**, there is very good agreement between the simulated and the experimental spectra. When moving from the isolated ZnPc to the dyad, the combined effect of the geometry change and the larger electron delocalization within the dyad results in the symmetry breaking and subsequent red shift of the Q band. The predicted red shift of the spectra for the exciton dyad is in very good agreement with the experiment. However, the energy splitting of the Q_x and Q_y transitions is slightly underestimated, which leads to a narrower Q band. For the **Dyad-PhA**, the results are very similar: the computed red shift from the **ZnPc-PhA** to the exciton dyad (60 cm^{-1}) is again very close to the experimental one (70 cm^{-1}).

For both systems, we also compared the exciton spectra with the spectra calculated on the full-QM dyads (see Figure S4 in the SI). For the full-QM dyad, there is a larger splitting of the

https://doi.org/10.1021/acsphyschemau.1c00049
ACS Phys. Chem Au 2022, 2, 206−215

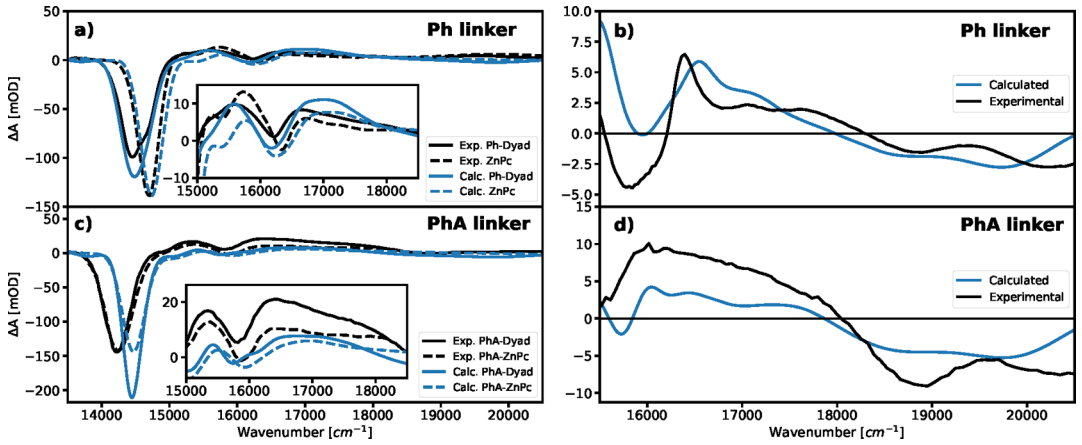

Figure 6. TA spectra for the dyads in toluene with the phenyl (upper part) and phenylamino linker (lower part). The left panels show the full spectra; the black lines correspond to the experiments, whereas the blue ones correspond to the simulated spectra. The spectrum of the **ZnPc-PhA** was shifted to have the same energy of the main ZnPc GSB peak as the **Dyad-PhA**, as was done for the experimental spectra in ref 16. The right panels show the difference spectra between the dyad and the ZnPc (or **ZnPc-PhA** for the case of the dyad with the phenylamine linker). The experimental spectra for the **Dyad-Ph** were obtained from ref 21 and those for **Dyad-PhA** from ref 16.

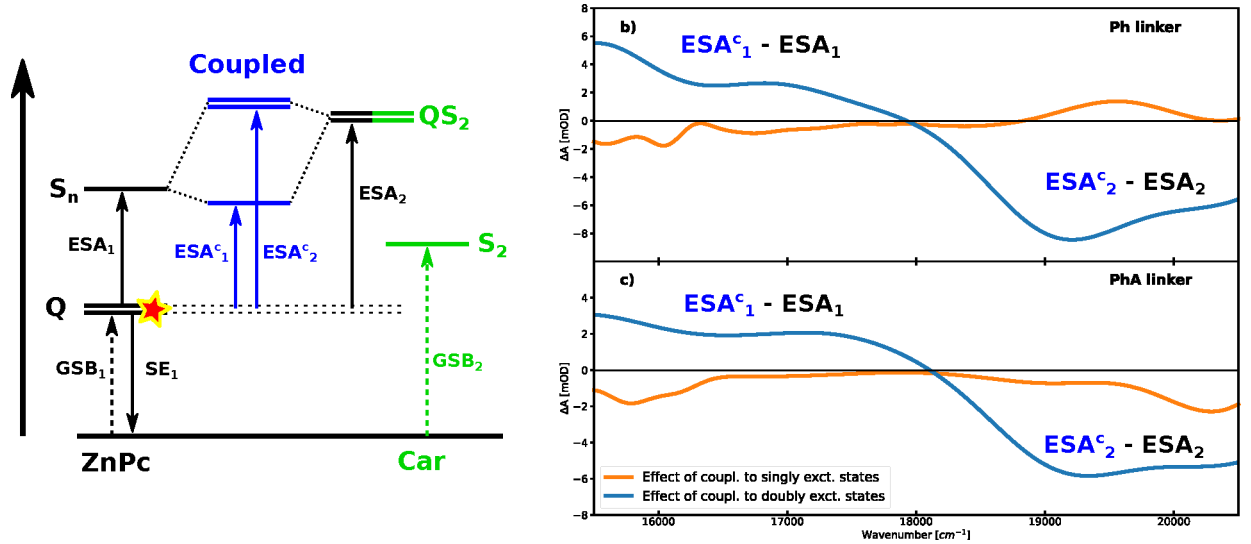

Figure 7. (a) Simplified scheme of signals observed after excitation of the $Q_{x/y}$ bands of the ZnPc moiety. The states S_3−S_{24} of the ZnPc are represented as a single S_n state for clarity. Effect of single-exciton and double-exciton couplings on the difference TA spectra for **Dyad-Ph** (b) and **Dyad-PhA** (c). The orange line represents the contribution of couplings among singly excited states only (i.e., doubly excited states are artificially decoupled), whereas the blue line represents the contribution due to couplings between the singly excited and doubly excited states $|Q_{x/y}^{\mathrm{ZnPc}} S_2^{\mathrm{Car}}\rangle$.

Q_x and Q_y states which leads to the broader Q band in agreement with the experiment. However, the computed red shift of the spectra for the full-QM dyads is overestimated by ∼200 cm^{-1} with respect to the experimental one. This overestimation can be imputed to the DFT functional here used (CAM-B3LYP), which may overestimate the electron delocalization in the dyads: this defect is automatically solved by introducing the exciton picture which, by construction, allows delocalization only within the fragments.

From the combined analysis of absorption spectra and electronic states, we can immediately see that the linker plays an important role in lowering transition energies and leading to slightly different orientations of the transition dipoles in the dyad diabatic states compared to the individual isolated fragments (Figure 4 and Table S1 in the SI). This issue complicates the analysis, because in the experiments the dyad is compared with the "individual fragments", but the electron delocalization makes it difficult to understand which are the correct separated fragments to consider.

Transient Absorption Spectra

Having defined and calculated the proper exciton Hamiltonians, we simulated the transient absorption spectra of the two dyads at a 2 ps delay time. In these calculations, we assume that the vibrational relaxation of the excited state has already taken place, but the system has not yet relaxed to the ground state.

In order to disentangle the effect of the Car S_1 state, we first present the simulated TA spectra obtained without including it. The experimental analysis of the signals was performed by subtracting the dyad and monomer TA spectra in both systems: in the case of the phenyl linker, the "monomer" corresponds to ZnPc,[19] while in the other case, the monomer is **ZnPc-PhA**.[16] We additionally note that, in ref 16, the spectrum of **ZnPc-PhA** was shifted to match the position of

https://doi.org/10.1021/acsphyschemau.1c00049
ACS Phys. Chem Au 2022, 2, 206−215

the Q band of the dyad. Our simulated spectra will be analyzed in the same way.

Figure 6a,c shows the comparison between experiments and calculations for the TA spectra of the two dyads and the corresponding ZnPc(-**PhA**) monomers. For **Dyad-Ph**, our calculations well reproduce the change in position and intensity of the main negative peak when passing from the monomer to the dyad (Figure 6a). The calculated dyad spectrum is slightly narrower, and therefore more intense, than the experimental one, due to a slightly smaller splitting of the Q_x and Q_y transitions. Also, the region between 15 000 and 18 000 cm^{-1} is well-reproduced by our calculations, although the ESA signal around 17 000 cm^{-1} is slightly overestimated. However, this contribution seems to be the same in both the ZnPc monomer and the dyad and will not affect the difference spectra. For **Dyad-PhA**, the situation is very similar (Figure 6c). A small blue shift is present with respect to the experiment; however, this does not affect the difference spectra and the spectral changes in the energy range >16 000 cm^{-1}.

The calculated difference spectra obtained by subtracting the monomer TA spectrum from that of the dyad are compared with the experiments in Figure 6b,d. We observe a generally good agreement, as the calculations reproduce the positive contribution in the 16 500−18 000 cm^{-1} range and the negative one above 18 000 cm^{-1}. Notably, our model reproduces this negative contribution without introducing the S_1 state. As we explain below, this signal arises from a complex interplay of exciton interactions in both the single-exciton and double-exciton manifolds.

As a matter of fact, multiple signals from different optical pathways contribute to the ∼16 000−22 000 cm^{-1} spectral region. A simplified scheme of these pathways is reported in Figure 7a.

After excitation, the $Q_{x/y}^{ZnPc}$ states are populated, and they contribute to the negative TA band at ∼14 500 cm^{-1} (GSB_1 and SE_1). In addition, there is a positive contribution (ESA_1) due to the $Q_{x/y}^{ZnPc} \rightarrow S_n^{ZnPc}$ transitions to the higher-lying states of ZnPc. These transitions contribute at 14 500−19 500 cm^{-1} to the TA spectrum.

As the Car S_0 band is found at ∼18 000−24 000 cm^{-1} (Figure 5), the GS → S_0 absorption will contribute a negative GSB signal in the spectrum (GSB_2). In the absence of exciton interactions between ZnPc and Car, this signal would be counterbalanced by the equal and opposite ESA_2 signal coming from the transition between the $Q_{x/y}^{ZnPc}$ and the doubly excited state $Q_{x/y}^{ZnPc}S_2^{Car}$. Exciton couplings mix the Car S_0 state with both the $Q_{x/y}$ and the S_n states of the ZnPc moiety. The overall effect of these single-exciton couplings on the difference TA spectrum is quite small, as shown in the orange plots of Figure 7b,c for **Dyad-Ph** and **Dyad-PhA**, respectively.

The largest effect comes from the doubly excited state $Q_{x/y}^{ZnPc}S_2^{Car}$, which mixes with the higher excited states of the ZnPc moiety, S_n^{ZnPc}. The new "coupled" transitions, ESA_1^c and ESA_2^c, have intensities that differ from the original ones. In fact, the $Q_{x/y} \rightarrow S_n$ transition of ZnPc (ESA_1^c) gains dipole strength at the expense of the $Q_{x/y}^{ZnPc} \rightarrow Q_{x/y}^{ZnPc}S_2^{Car}$ transition (ESA_2^c) (see Section S7 in the SI). These couplings between single and double exciton states significantly affect the difference TA spectrum, as shown in Figure 7b,c (blue lines). Indeed, these contributions perfectly explain both the positive TA difference below 18 000 cm^{-1} and the negative signal at higher frequencies.

Finally, the additional differential signal around 16 000 cm^{-1} arises from the geometry change of the ZnPc moiety when passing from the monomer to the dyad and from adding the Ph linker to the ZnPc for the case of **Dyad-Ph** (Figure S5 in the SI). For **Dyad-PhA**, this contribution is much lower than for **Dyad-Ph**, because the dyad is compared with **ZnPc-PhA** which has a geometry very similar to that of the dyad.

For **Dyad-PhA**, the agreement is not as good as for **Dyad-Ph**; however, the simulated spectra qualitatively explain the observed spectral changes. The negative signal agrees quantitatively well with the experimental results; however, the positive signal is underestimated, which is also seen in the TA spectra of both **ZnPc-PhA** and the dyad. Even if our calculations do not quantitatively explain the positive contribution, we can explain the origin of both negative and positive signals without including the Car S_1 state. In addition, when the Car excitation energy is slightly blue-shifted to obtain better agreement with the experimental linear absorption spectra, the model also precisely determines the position of the zero-crossing (see Section S7 in the SI).

From this analysis, it comes out that the measured difference spectra can be explained without introducing the effect of the Car S_1 state. Instead, our results provide an alternative explanation of the observed signals, which does not require an exciton delocalization between ZnPc and the Car S_1 state while it introduces the possibility of a coupling between the ZnPc higher excited states with the doubly excited state $|Q_{x/y}^{ZnPc}S_2^{Car}\rangle$. To the best of our knowledge, this hypothesis has been so far neglected in all spectroscopic models of the dyads.

Notably, the transitions here discussed occur when the dyad is in the $Q_{x/y}$ states localized on the ZnPc part. Therefore, the signal in the TA difference appears immediately after excitation of the $Q_{x/y}$ states and does not require the population of excited states localized on the Car moiety. In addition, this signal evolves with the $Q_{x/y}$ population. As the ESA_2/ESA_2^c signals have the same line shape as the $S_0 \rightarrow S_2$ Car transition, they can be easily mistaken for a GSB of the Car S_2 absorption.

Effect of the Car S_1 State

Up to now, we have given an explanation of the TA signals without considering the Car dark S_1 state in the spectral simulations. Now, we can check what would change by including this state in our model. In order to assess the effects of the S_1 state, we estimated its contribution to the spectra through the exciton mixing with the ZnPc Q states. The excitation energy and vibronic coupling of the S_1 state are inaccessible to the TD-DFT approach due to its predominantly double excitation character and are extremely difficult to compute even with accurate multireference methods. We estimated the vertical absorption energy and the vibronic parameters from two-photon absorption (TPA) and fluorescence data.[20,26] The S_1 state vibronic progression can be described with a single effective frequency (ω_{S1} = 1400 cm^{-1}) as previously done, e.g., in ref 27. From the fitting of the TPA spectra, we obtained the S_1 0−0 transition energy at 14 200 cm^{-1} and the reorganization energy for the vibrational mode λ_{S1} = 8970 cm^{-1}. More details about the fitting procedure can be found in Section S8.1 in the Supporting Information.

The last missing quantity needed to estimate the exciton mixing of S_1 with the Q states is the exciton coupling. Even if the S_1 state of carotenoids has a predominantly double excitation character, a non-negligible single excitation contribution is present.[28] It is exactly this contribution that

https://doi.org/10.1021/acsphyschemau.1c00049
ACS Phys. Chem Au 2022, 2, 206−215

determines the transition density, which we use in combination with the TDC method to compute the coupling with Q_x. We therefore calculated the S_1 transition density at the TD-DFT level using CAM-B3LYP (Figure S8 in the SI). The resulting coupling is $V^{TDC}_{S_1-Q_x}$ = 97 cm^{-1}.

To check the accuracy of such a coupling, we computed transfer rates and corresponding lifetimes and compared them with experiments. As the exciton coupling between Car S_1 and ZnPc Q states is much smaller than the reorganization energy, the system falls into the Förster regime of energy transfer.[29−31] For the calculation of the transfer rates, the S_1 state was described as a single electronic transition with all of the vibrations included in the spectral density with the reorganization energy λ_{S_1}. For this model, the vertical excitation energy $\varepsilon_{S_1} = \varepsilon^{0-0}_{S_1} + \lambda_{S_1}$ is used for computing the Förster transfer rates (see Section S3 in the SI). The resulting lifetime of the Q states τ = 66 ps agrees very well with the experimental lifetime of 67 ps.[16]

To check the robustness of this result, we repeated the same calculations for dyads containing carotenoids with different conjugation lengths, namely, 8 and 11 double bonds (DB). The calculated electronic couplings and the estimated energetic parameters used for the different dyads are reported in Table 1. The resulting calculated lifetimes agree well with the experimental ones for the whole series of dyads.[16] To obtain a confidence interval for our computed lifetimes, we repeated the calculations using a range of S_1 excitation energies (12 000−17 000 cm^{-1}) and a range of reorganization energies ±1000 cm^{-1} from the fitted one. If we combine these results (reported in Figure S9 in the SI) with the experimental inaccuracy of the 0−0 excitation energy (±350 cm^{-1}), we finally obtain the confidence intervals for our computed lifetimes reported in Table 1. As can be seen, for all dyads, the computed intervals of lifetimes contain the experimentally estimated values.

Table 1. Comparison of Calculated and Experimental Lifetimes τ for the Excitation Transfer from the ZnPc-Ph Q to the Car S_1 State for Three Dyads with Carotenoids of Different Conjugation Lengths in Toluene Solvent[a]

Car in Dyad	$V^{TDC}_{S_1-Q_x}$ (cm^{-1})	λ_{S_1} (cm^{-1})	$\varepsilon^{0-0}_{S_1}$ (cm^{-1})	τ^{calc} (ps)	τ^{exp} (ps)
8 DB	106	6216	15 600	454 [109, 813]	327
10 DB	97	8970	14 200	66 [55, 77]	67
11 DB	76	8970	13 500	38 [20, 87]	29

[a]The electronic couplings ($V^{TDC}_{S_1-Q_x}$) are given, together with the estimated 0−0 excitation energies ($\varepsilon^{0-0}_{S_1}$) and reorganization energies (λ_{S_1}) of the S_1 state (see Section S8.1 in the Supporting Information). The values in brackets correspond to a confidence interval for the lifetimes based on the experimental inaccuracy of ±350 cm^{-1} for the Car S_1 vibronic transition energies (ref 20). The experimental lifetimes were obtained from the TA spectra.[16]

The good results obtained in the checks on the accuracy and robustness of the exciton coupling allow us to proceed further in the investigation of the effects of the exciton mixing between the Car S_1 state and the ZnPc Q states.

Here, we are mainly interested in the coupling of the individual 0−0 transitions, which are energetically close. The calculated coupling thus has to be scaled by the Franck−Condon factor of the Car vibrational transition, obtaining $V^{TDC,0-0}_{S_1-Q_x}$ = 4 cm^{-1} (see Section S2.1 in the SI). Based on the experimental S_1 transition energy, the energy difference between 0 and 0 transition energies ($\Delta\varepsilon^{0-0} = \varepsilon^{0-0}_{Q_x} - \varepsilon^{0-0}_{S_1}$ = 277 cm^{-1}) leads to an exciton mixing with a negligible (0.02%) contribution of the Car S_1 state. We note that the higher vibronic states have larger FC factors and therefore also larger couplings, but they also have a too large energy gap which again leads to a negligible exciton mixing.

To estimate the S_1 contribution needed to explain the observed positive peak for the lowest allowed state of the dyad in the difference spectra, we extracted the S_1 ESA signal from the TA experiments of the isolated Car. The spectra were then renormalized to match the intensity of the Car S_2 absorption peak in the isolated Car and the dyad. The resulting contribution is shown alongside the difference TA spectra in Figure S10 in the SI. We see that a ∼20% contribution of the Car S_1 state is needed to explain the observed data in terms of the exciton mixing between Car and ZnPc. In order to obtain such a large contribution, the coupling between 0 and 0 transitions should be in the order of ∼190 cm^{-1}, which is unrealistically high even if we consider that our fit might underestimate the Franck−Condon factor for the 0−0 transition. We can therefore conclude that a large exciton mixing between the Car S_1 state and ZnPc Q band is improbable and that the observed difference signal is more likely due to the exciton mixing of higher ZnPc states with the doubly excited state of the dyad.

All of these results also suggest that EET from the ZnPc to the Car S_1 state is not mediated by exciton mixing. For an apolar solvent like toluene, we can also rule out transfer through the charge transfer state, whose signature is experimentally observed only in polar solvents.[14,16] These findings support our hypothesis that the ZnPc to Car excitation transfer is, for the two investigated dyads, mostly due to a "hopping" mechanism more than an exciton mixing. The experimentally observed bidirectional transfer for the Car with 10 DB in the conjugated chain[17,20] can be explained by the small energy gap (∼277 cm^{-1}) between 0 and 0 transitions of Car S_1 and ZnPc Q_x states, without invoking exciton mixing as previously suggested.[16,19,21]

CONCLUDING REMARKS

Covalent dyads containing tetrapyrroles and carotenoids have found a use as "minimal" model systems to infer implications on the mechanisms of NPQ and photoregulation.[22] However, here, we have shown that this analysis is less straightforward than generally thought.

By using quantum mechanical calculations, we have characterized the exciton structure of two covalently linked dyads containing a Zn phthalocyanine and a carotenoid and computed their linear and transient absorption spectra.

We have shown that the exciton structure of the two dyads cannot be easily disentangled as the interaction between two independent monomers, because the linkers participate in the electronic delocalization of both the Car and the ZnPc transitions. For the Car, the GS → S_2 electronic transition is invariably delocalized in the linker. The latter also breaks the symmetry of the ZnPc, splitting the two Q states and changing their transition dipoles. Thus, the linker has to be considered as a part of both monomers.

https://doi.org/10.1021/acsphyschemau.1c00049
ACS Phys. Chem Au 2022, 2, 206−215

The calculated transient absorption spectra imply a different explanation for the characteristic features previously assigned to exciton coupling between the phthalocyanine Q states and the Car S_1 state. According to our results, in fact, those signals arise from a complex interplay of exciton couplings involving higher-lying singly and doubly excited states. These couplings affect the intensity of both ground-state bleaching and excited-state absorption in the broad 16 000−20 000 cm^{-1} spectral region, creating an apparent S_1 signal.

We finally show that the electronic coupling between the S_1 state and the Q states, although too small to result in any exciton mixing of these two states and to influence the TA spectra, is sufficient to explain the observed Förster $Q \rightarrow S_1$ EET rates.

COMPUTATIONAL DETAILS

The excited-state properties and transition dipoles of the dyads were modeled using the Frenkel exciton model formalism with the vibronic basis.[27,32,33] In this approach, the vibrational modes with the highest coupling to electronic transitions are included in the exciton Hamiltonian. The resulting exciton states can be obtained from diagonalization of the following Hamiltonian:

$$H = \sum_{\nu\eta}\sum_{i,j}(\varepsilon_i + \varepsilon_j^{(0-0)} + \nu\omega_1 + \eta\omega_2)|ij_{\nu\eta}\rangle\langle ij_{\nu\eta}| + \sum_{\nu\eta\kappa\xi}\sum_{\substack{i\neq j\\ k\neq l}} V_{ij_{\nu\eta},kl_{\kappa\xi}}|ij_{\nu\eta}\rangle\langle kl_{\kappa\xi}| \quad (1)$$

where i corresponds to the electronic state of the zinc-phthalocyanine, j to the electronic state of the carotenoid; ν and κ are quantum numbers of the first vibrational mode with frequency ω_1, and η and ξ are quantum numbers of the second vibrational mode with frequency ω_2. These modes correspond to the Car C—C and C═C stretching[34] (Section S5.2 in the SI). ε_i is the vertical excitation energy of the ZnPc from the ground to the excited state i, and ε_j^{0-0} is the 0−0 electronic transition energy of the Car jth electronic state. The Hamiltonian in eq 1 contains both singly excited states (where $i = 0$ or $j = 0$) and doubly excited states ($i, j \neq 0$). The coupling $V_{ij_{\nu\eta},kl_{\kappa\xi}}$ between vibronic states $|ij_{\nu\eta}\rangle$ and $|kl_{\kappa\xi}\rangle$ is computed as detailed in Section S2.1 of the Supporting Information.

All of the quantities needed for the exciton model were calculated with Gaussian 16 software.[35] The ground-state geometries were optimized using a DFT description with the B3LYP functional[36] and 6-31G(d,p) basis set. The DFT functional and basis set were chosen based on the good agreement of the IR and Raman spectra with the experimental ones among other tested functionals CAM-B3LYP[37] and ωB97X-D[38] (see Section S1 of the SI). The excited-state properties were obtained within the TD-DFT approach with the CAM-B3LYP functional and the same basis set as for the geometry optimization. For Car, the 5 lowest excited states were computed whereas, for ZnPc and Dyad, 24 excited states and 36 excited states, respectively, were computed. The effects of the toluene solvent used in the experiments were included within the Integral Equation Formalism (IEF)[39] of the Polarizable Continuum Model (PCM)[40] for both the conformational analysis and the calculation of the excitation properties. For the calculation of conformational populations, we used the PCM free energies calculated using the default model implemented in Gaussian. Transition energies and properties were computed with the nonequilibrium linear response solvation, and a state-specific correction was introduced for each excitation using the corrected linear response (cLR) approach.[41,42]

The diabatization of the dyad was performed using the multistate FCD-FED algorithm[43] with the basis of 18 excited states of the dyad computed with the CAM-B3LYP functional. We set the individual fragments of the dyad for the diabatization algorithm by cutting the single bond between the phenyl linker and ZnPc. The dangling bond after the cut of the dyad into the individual monomers was capped with a hydrogen atom. The excited states of the **ZnPc-Ph(A)** and **Car-Ph** for the dyad calculations were computed at the B3LYP optimized geometry of the dyad. The exciton coupling between individual monomers was computed with the transition density cube (TDC) method[25]

To reproduce the TA spectra, it is very important to have accurate excitation energies. Because TD-DFT generally describes the lowest excited states with a better accuracy than the higher excited states, two different energy shifts were applied to correct this intrinsic error of the TD-DFT approach. The lowest ZnPc states (first to fifth excited state) as well as the Car S_2 state were consistently shifted by −0.156 eV to match the experimental position of the first ZnPc absorption peak. The higher excited states of the ZnPc (starting from the sixth excited state) were consistently shifted by −0.540 eV to obtain the Soret band at the experimental position of the ZnPc second absorption peak.

The transient absorption spectra were simulated at the excited-state thermal equilibrium. In the experiments, this equilibrium is reached after 2 ps when the spectra do not undergo any fast changes and only present a slow decrease of the intensity due to excitation transfer and relaxation to the ground state. In the excited-state thermal equilibrium, we assume that the system is in the vibrational ground state of the lowest exciton states. The population of the lowest exciton states was determined from the Boltzmann distribution at room temperature. All spectra were computed within the exciton model and in the cumulant expansion formalism.[44,45] A more detailed description of the model used for simulating the absorption and TA spectra can be found in Section S2 of the Supporting Information.

ASSOCIATED CONTENT

Supporting Information

The Supporting Information is available free of charge at https://pubs.acs.org/doi/10.1021/acsphyschemau.1c00049.

Comparison of DFT functionals for ground-state optimization and normal-mode analysis; details of the exciton model and optical spectra calculation; Förster model for computing the excitation energy transfer rates; correction for the different DFT functionals for computing the ground-state properties and the excited-state gradients for the spectral density; details of the optical parameters for the individual ZnPc and Car monomers; comparison between the exciton and full QM model of the dyads; additional details about the origin of the signal in the difference spectra between the dyad and the ZnPc monomer; and details of the fitting of the Car S_1 state optical properties and computing the Förster rates (PDF)

https://doi.org/10.1021/acsphyschemau.1c00049
ACS Phys. Chem Au 2022, 2, 206−215

AUTHOR INFORMATION

Corresponding Authors

Vladislav Sláma − *Dipartimento di Chimica e Chimica Industriale, University of Pisa, 56124 Pisa, Italy;* Email: vladislav.slama@dcci.unipi.it

Benedetta Mennucci − *Dipartimento di Chimica e Chimica Industriale, University of Pisa, 56124 Pisa, Italy;* orcid.org/0000-0002-4394-0129; Email: benedetta.mennucci@unipi.it

Author

Lorenzo Cupellini − *Dipartimento di Chimica e Chimica Industriale, University of Pisa, 56124 Pisa, Italy;* orcid.org/0000-0003-0848-2908

Complete contact information is available at: https://pubs.acs.org/10.1021/acsphyschemau.1c00049

Notes

The authors declare no competing financial interest.

ACKNOWLEDGMENTS

The authors acknowledge funding by the European Research Council, under Grant ERC-AdG-786714 (LIFETimeS).

REFERENCES

(1) Polívka, T.; Frank, H. A. Molecular Factors Controlling Photosynthetic Light Harvesting by Carotenoids. *Acc. Chem. Res.* **2010**, *43*, 1125−1134.

(2) Müller, P.; Li, X. P.; Niyogi, K. K. Non-photochemical quenching. A response to excess light energy. *Plant Physiology* **2001**, *125*, 1558−1566.

(3) Pascal, A. A.; Liu, Z.; Broess, K.; Van Oort, B.; Van Amerongen, H.; Wang, C.; Horton, P.; Robert, B.; Chang, W.; Ruban, A. Molecular basis of photoprotection and control of photosynthetic light-harvesting. *Nature* **2005**, *436*, 134−137.

(4) Li, Z.; Wakao, S.; Fischer, B. B.; Niyogi, K. K. Sensing and Responding to Excess Light. *Annu. Rev. Plant Biol.* **2009**, *60*, 239−260.

(5) Ruban, A. V.; Johnson, M. P.; Duffy, C. D. The Photoprotective Molecular Switch in the Photosystem II Antenna. *Biochim. Biophys. Acta - Bioenerg.* **2012**, *1817*, 167−181.

(6) Niyogi, K. K.; Truong, T. B. Evolution of flexible non-photochemical quenching mechanisms that regulate light harvesting in oxygenic photosynthesis. *Curr. Opin. Plant Bio.* **2013**, *16*, 307−314.

(7) Nicol, L.; Nawrocki, W. J.; Croce, R. Disentangling the sites of non-photochemical quenching in vascular plants. *Nat. Plants* **2019**, *5*, 1177−1183.

(8) Pinnola, A.; Bassi, R. Molecular mechanisms involved in plant photoprotection. *Biochem. Soc. Trans.* **2018**, *46*, 467−482.

(9) van Oort, B.; van Hoek, A.; Ruban, A. V.; van Amerongen, H. Equilibrium between Quenched and Nonquenched Conformations of the Major Plant Light-Harvesting Complex Studied with High-Pressure Time-Resolved Fluorescence. *J. Phys. Chem. B* **2007**, *111*, 7631−7637.

(10) Krüger, T. P. J.; Wientjes, E.; Croce, R.; Grondelle, R. v. Conformational switching explains the intrinsic multifunctionality of plant light-harvesting complexes. *Proc. Natl. Acad. Sci. U. S. A.* **2011**, *108*, 13516−13521.

(11) Schlau-Cohen, G. S.; Yang, H. Y.; Krüger, T. P. J.; Xu, P.; Gwizdala, M.; Van Grondelle, R.; Croce, R.; Moerner, W. E. Single-molecule identification of quenched and unquenched states of LHCII. *J. Phys. Chem. Lett.* **2015**, *6*, 860−867.

(12) Kondo, T.; Pinnola, A.; Chen, W. J.; Dall'Osto, L.; Bassi, R.; Schlau-Cohen, G. S. Single-molecule spectroscopy of LHCSR1 protein dynamics identifies two distinct states responsible for multi-timescale photosynthetic photoprotection. *Nat. Chem.* **2017**, *9*, 772−778.

(13) Cignoni, E.; Lapillo, M.; Cupellini, L.; Acosta-Gutiérrez, S.; Gervasio, F. L.; Mennucci, B. A different perspective for non-photochemical quenching in plant antenna complexes. *Nat. Commun.* **2021**, *12*, 7152.

(14) Berera, R.; Herrero, C.; van Stokkum, I. H. M.; Vengris, M.; Kodis, G.; Palacios, R. E.; van Amerongen, H.; van Grondelle, R.; Gust, D.; Moore, T. A.; et al. A simple artificial light-harvesting dyad as a model for excess energy dissipation in oxygenic photosynthesis. *Proc. Natl. Acad. Sci. U. S. A.* **2006**, *103*, 5343−5348.

(15) Berera, R.; Grondelle, R. v.; Kennis, J. T. M. Ultrafast transient absorption spectroscopy: principles and application to photosynthetic systems. *Photosynth. Res.* **2009**, *101*, 105−118.

(16) Kloz, M.; Pillai, S.; Kodis, G.; Gust, D.; Moore, T. A.; Moore, A. L.; van Grondelle, R.; Kennis, J. T. M. Carotenoid Photoprotection in Artificial Photosynthetic Antennas. *J. Am. Chem. Soc.* **2011**, *133*, 7007−7015.

(17) Liao, P.-N.; Pillai, S.; Gust, D.; Moore, T. A.; Moore, A. L.; Walla, P. J. Two-Photon Study on the Electronic Interactions between the First Excited Singlet States in Carotenoid-Tetrapyrrole Dyads. *J. Phys. Chem. A* **2011**, *115*, 4082−4091.

(18) Pillai, S.; Ravensbergen, J.; Antoniuk-Pablant, A.; Sherman, B. D.; Grondelle, R. v.; Frese, R. N.; Moore, T. A.; Gust, D.; Moore, A. L.; Kennis, J. T. M. Carotenoids as electron or excited-state energy donors in artificial photosynthesis: an ultrafast investigation of a carotenoporphyrin and a carotenofullerene dyad. *Phys. Chem. Chem. Phys.* **2013**, *15*, 4775.

(19) Maiuri, M.; Snellenburg, J. J.; van Stokkum, I. H. M.; Pillai, S.; WongCarter, K.; Gust, D.; Moore, T. A.; Moore, A. L.; van Grondelle, R.; Cerullo, G.; et al. Ultrafast Energy Transfer and Excited State Coupling in an Artificial Photosynthetic Antenna. *J. Phys. Chem. B* **2013**, *117*, 14183−14190.

(20) Gacek, D. A.; Moore, A. L.; Moore, T. A.; Walla, P. J. Two-Photon Spectra of Chlorophylls and Carotenoid−Tetrapyrrole Dyads. *J. Phys. Chem. B* **2017**, *121*, 10055−10063.

(21) Ravensbergen, J.; Pillai, S.; Méndez-Hernández, D. D.; Frese, R. N.; van Grondelle, R.; Gust, D.; Moore, T. A.; Moore, A. L.; Kennis, J. T. M. Dual Singlet Excited-State Quenching Mechanisms in an Artificial Caroteno-Phthalocyanine Light Harvesting Antenna. *ACS Phys. Chem. Au* **2022**, *2* (1), 59−67.

(22) Liao, P.-N.; Pillai, S.; Kloz, M.; Gust, D.; Moore, A. L.; Moore, T. A.; Kennis, J. T. M.; van Grondelle, R.; Walla, P. J. On the role of excitonic interactions in carotenoid−phthalocyanine dyads and implications for photosynthetic regulation. *Photosynth. Res.* **2012**, *111*, 237−243.

(23) Renger, T. Theory of excitation energy transfer: from structure to function. *Photosynth. Res.* **2009**, *102*, 471−485.

(24) Tavan, P.; Schulten, K. Electronic excitations in finite and infinite polyenes. *Phys. Rev. B* **1987**, *36*, 4337−4358.

(25) Krueger, B. P.; Scholes, G. D.; Fleming, G. R. Calculation of Couplings and Energy-Transfer Pathways between the Pigments of LH2 by the ab Initio Transition Density Cube Method. *J. Phys. Chem. B* **1998**, *102*, 5378−5386.

(26) Gillbro, T.; Andersson, P. O.; Liu, R. S. H.; Asato, A. E.; Takaishi, S.; Cogdell, R. J. Location of the Carotenoid 2Ag-state and its Role in Photosynthesis. *Photochem. Photobio.* **1993**, *57*, 44−48.

(27) Perlík, V.; Seibt, J.; Cranston, L. J.; Cogdell, R. J.; Lincoln, C. N.; Savolainen, J.; Šanda, F.; Mančal, T.; Hauer, J. Vibronic coupling explains the ultrafast carotenoid-to-bacteriochlorophyll energy transfer in natural and artificial light harvesters. *J. Chem. Phys.* **2015**, *142*, 212434.

(28) Bondanza, M.; Jacquemin, D.; Mennucci, B. Excited States of Xanthophylls Revisited: Toward the Simulation of Biologically Relevant Systems. *J. Phys. Chem. Lett.* **2021**, *12*, 6604−6612.

(29) Förster, T. Zwischenmolekulare Energiewanderung und Fluoreszenz. *Ann. Phys.* **1948**, *437*, 55−75.

(30) Chenu, A.; Scholes, G. D. Coherence in Energy Transfer and Photosynthesis. *Annu. Rev. Phys. Chem.* **2015**, *66*, 69−96.

(31) May, V.; Kühn, O. *Charge and Energy Transfer Dynamics in Molecular Systems*; John Wiley & Sons, Ltd: Weinheim, Germany, 2011; Chapter 9, pp 467−558.
(32) Polyutov, S.; Kühn, O.; Pullerits, T. Exciton-vibrational coupling in molecular aggregates: Electronic versus vibronic dimer. *Chem. Phys.* **2012**, *394*, 21−28.
(33) Butkus, V.; Valkunas, L.; Abramavicius, D. Vibronic phenomena and exciton−vibrational interference in two-dimensional spectra of molecular aggregates. *J. Chem. Phys.* **2014**, *140*, 034306.
(34) Polívka, T.; Sundström, V. Ultrafast Dynamics of Carotenoid Excited States - From Solution to Natural and Artificial Systems. *Chem. Rev.* **2004**, *104*, 2021−2072.
(35) Frisch, M. J.; Trucks, G. W.; Schlegel, H. B.; Scuseria, G. E.; Robb, M. A.; Cheeseman, J. R.; Scalmani, G.; Barone, V.; Petersson, G. A.; Nakatsuji, H.; Li, X.; Caricato, M.; Marenich, A. V.; Bloino, J.; Janesko, B. G.; Gomperts, R.; Mennucci, B.; Hratchian, H. P.; Ortiz, J. V.; Izmaylov, A. F.; Sonnenberg, J. L.; Williams-Young, D.; Ding, F.; Lipparini, F.; Egidi, F.; Goings, J.; Peng, B.; Petrone, A.; Henderson, T.; Ranasinghe, D.; Zakrzewski, V. G.; Gao, J.; Rega, N.; Zheng, G.; Liang, W.; Hada, M.; Ehara, M.; Toyota, K.; Fukuda, R.; Hasegawa, J.; Ishida, M.; Nakajima, T.; Honda, Y.; Kitao, O.; Nakai, H.; Vreven, T.; Throssell, K.; Montgomery, J. A., Jr.; Peralta, J. E.; Ogliaro, F.; Bearpark, M.; Heyd, J. J.; Brothers, E. N.; Kudin, K. N.; Staroverov, V. N.; Kobayashi, R.; Normand, J.; Raghavachari, K.; Rendell, A.; Burant, J. C.; Iyengar, S. S.; Tomasi, J.; Cossi, M.; Millam, J. M.; Klene, M.; Adamo, C.; Cammi, R.; Ochterski, J. W.; Martin, R. L.; Morokuma, K.; Farkas, O.; Foresman, J. B.; Fox, D. J. *Gaussian 16*, revision A.03; Gaussian, Inc.: Wallingford CT, 2016.
(36) Becke, A. D. Density-functional thermochemistry. III. The role of exact exchange. *J. Chem. Phys.* **1993**, *98*, 5648−5652.
(37) Yanai, T.; Tew, D. P.; Handy, N. C. A new hybrid exchange−correlation functional using the Coulomb-attenuating method (CAM-B3LYP). *Chem. Phys.s Lett.* **2004**, *393*, 51−57.
(38) Chai, J.-D.; Head-Gordon, M. Long-range corrected hybrid density functionals with damped atom−atom dispersion corrections. *Phys. Chem. Chem. Phys.* **2008**, *10*, 6615−6620.
(39) Cancès, E.; Mennucci, B.; Tomasi, J. A new integral equation formalism for the polarizable continuum model: Theoretical background and applications to isotropic and anisotropic dielectrics. *J. Chem. Phys.* **1997**, *107*, 3032−3041.
(40) Tomasi, J.; Mennucci, B.; Cammi, R. Quantum Mechanical Continuum Solvation Models. *Chem. Rev.* **2005**, *105*, 2999−3094.
(41) Caricato, M.; Mennucci, B.; Tomasi, J.; Ingrosso, F.; Cammi, R.; Corni, S.; Scalmani, G. Formation and relaxation of excited states in solution: A new time dependent polarizable continuum model based on time dependent density functional theory. *J. Chem. Phys.* **2006**, *124*, 124520.
(42) Guido, C. A.; Chrayteh, A.; Scalmani, G.; Mennucci, B.; Jacquemin, D. Simple Protocol for Capturing Both Linear-Response and State-Specific Effects in Excited-State Calculations with Continuum Solvation Models. *J. Chem. Theory Comput.* **2021**, *17*, 5155−5164.
(43) Nottoli, M.; Jurinovich, S.; Cupellini, L.; Gardiner, A. T.; Cogdell, R.; Mennucci, B. The role of charge-transfer states in the spectral tuning of antenna complexes of purple bacteria. *Photosynth. Res.* **2018**, *137*, 215−226.
(44) Abramavicius, D.; Palmieri, B.; Voronine, D. V.; Šanda, F.; Mukamel, S. Coherent Multidimensional Optical Spectroscopy of Excitons in Molecular Aggregates; Quasiparticle versus Supermolecule Perspectives. *Chem. Rev.* **2009**, *109*, 2350−2408.
(45) Mukamel, S. *Principles of Nonlinear Optical Spectroscopy*; Oxford University Press, 1995.

https://doi.org/10.1021/acsphyschemau.1c00049
ACS Phys. Chem Au 2022, 2, 206−215